Tensile bifurcations in a truncated hemispherical thin elastic shell

Ciprian D. Coman[1†]

[1] *Department of Computer Science, School of Computing & Engineering, University of Huddersfield, HD1 3DH, Huddersfield, UK*

4 September 2020

Abstract

The work described in this paper is concerned with providing a rational asymptotic analysis of the wrinkling bifurcation experienced by a thin elastic hemispherical segment subjected to vertical tensile forces on its upper rim. This is achieved by considering the interplay between two boundary layers and matching the corresponding solutions associated with each separate region. Our key result is a four-term asymptotic formula for the critical load in terms of a small parameter proportional to the ratio between the thickness and the radius of the shell. Comparisons of this formula with direct numerical simulations provide further insight into the range of validity of the results derived herein.

Keywords: wrinkling, boundary layers, shallow shell equations, matched asymptotics.

[†] cdc3p@yahoo.com

1 Introduction

The mechanical failure of structural elements under tensile loading is arguably far less common than in the case of compressive forces. It is therefore unsurprising that despite a vast literature on elastic buckling, the role played by tensile forces in triggering elastic instabilities is much less well documented. Perhaps, one of the possible explanations for the scarcity of this latter topic has to do with the fact that *compressive* stresses are not always triggered in structures subjected to tensile loads. When they do, such stresses are usually part of inhomogeneous stress fields that lead to bifurcation equations with variable coefficients, and whose analytical solutions tend to lie beyond the scope of most engineering curricula.

In recent years there has been a resurgence of interest in the onset of buckling-type instabilities in thin elastic plates under tension (e.g., [1, 2, 3, 4, 5, 6]). Such interest has been mainly driven by various practical applications (e.g., [7, 8, 9, 10]) and has generated many new insights into such an old and well-plowed field as elastic buckling. On the other hand, examples of buckling in thin shells subjected to tensile forces have attracted comparatively less attention, although there are a number of common configurations known to be prone to such instabilities. An example in this direction is that of a truncated hemispherical shell subjected to vertical pulling forces uniformly distributed on its upper rim, and clamped along the equator. Yao [11] was the first to take up a brief numerical and experimental exploration of this interesting problem. He noted that the buckled shape was similar to that of a cylinder buckled under radial pressure, consisting of one axial half-wave and a short-wavelength rippling pattern around the shell's lateral surface (i.e., in the azimuthal direction). Although his numerical work was based on a rather crude Galerkin method, he managed to obtain reasonably accurate values for the critical tension responsible for the instability. The starting point of this numerical work was a simplified version of the shallow-shell equations (e.g., [12, 13]) linearised around a membrane basic state; it is well known that the linear membrane solution for this type of configuration yields azimuthal compressive stresses throughout the entire shell (for example, see [14, 15]), and hence represents the cause of the rippling deformation pattern observed in experiments.

Yao's study was re-visited by Bushnell [16] (see also [17]) a few years later, as part of a larger investigation dealing with spherical shells subjected to concentrated and ring loads. His basic state was described by Reissner's simplified nonlinear axisymmetric equations for small "finite" rotations (see equations (III) and (IV) in [18]), and shallow-shell theory was used to identify possible neutrally stable equilibrium states superimposed on the rotationally symmetric solution (cf. [19, 20]). Bushnell dealt with a wide range of configurations, like the one seen in Figure 1, which includes the truncated hemisphere as a special case ($\phi_2 \equiv 90^\circ$ and $0 < \phi_1 < 90^\circ$). He discovered that the buckling deformation is confined near the edge at ϕ_1 for $\phi_1 < 52^\circ$, while buckling loads are independent of ϕ_2 for sufficiently large $\phi_2 - \phi_1$. Rather unexpectedly, it was also found that the validity of the linear membrane basic state holds true for an extensive set of ϕ_1-values, particularly as the radius-to-thickness ratio increases. However, for $\phi_1 < 11.5^\circ$ the predictions of the nonlinear theory suggested buckling with a larger number of circumferential waves than in the linear case. Based on his numerical data Bushnell proposed a couple of simplified formulae for the critical load as well as the number of wrinkles; these were derived by ad-hoc methods and captured quite well the dependence on the radius-to-thickness parameter already mentioned above.

Most of the subsequent studies that re-visited the truncated hemisphere under tension dealt with it marginally by treating Yao's configuration more like an example, or as an illustration of a specific technique, rather than for its own intrinsic interest. For example, Budiansky and Hutchinson [21, 22] were mostly interested in the imperfection sensitivity of toroidal shell segments and other non-standard shell configurations, while Navaratna *et al.* [23] used Yao's numerical solution as a benchmark

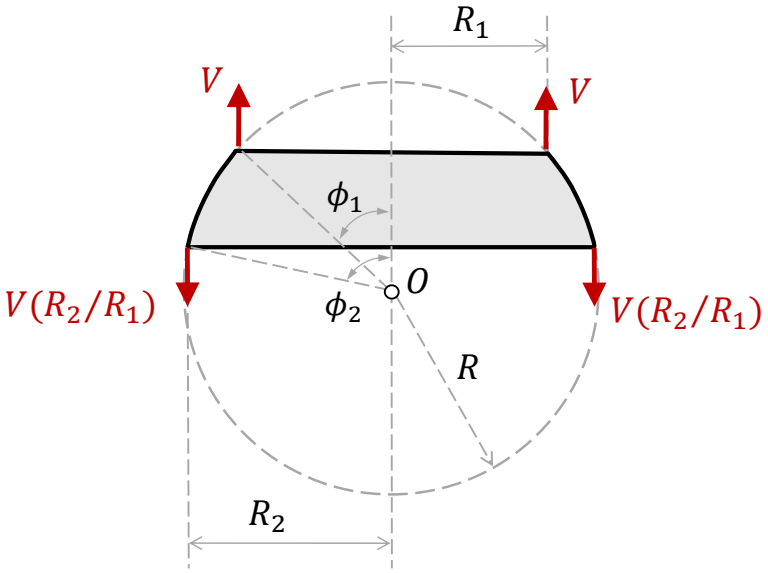

Figure 1: Side view of a *spherical shell segment* subjected to vertical tensile forces on its upper rim ($R_1 < R_2 \leq R$); this corresponds to the configuration studied numerically in [16].

for testing the suitability of their finite-element displacement method to buckling problems. Wu and Cheng [24] adopted the well-known Sanders' nonlinear shell theory [25] to derive an extremely complicated set of buckling equations in displacements, which used a nonlinear axisymmetric basic state employing the same type of kinematics. These equations were then solved numerically by using finite-difference methods and yielded critical loads very close to those reported previously in [11]. Wu and Cheng's results demonstrated clearly that differences between the original linear membrane solution and their nonlinear bending basic state were limited to the edges of the shell, with the eigenmodes being situated mostly outside of those regions (see Figures 5-7 in their work). Radhamohan and Prasad [26] used the same Sanders' nonlinear equations (but re-arranged differently) to derive their buckling equations for a toroidal shell under axial tension. They used this problem as an illustration of the parametric differentiation technique for the numerical solution of nonlinear shell equations, and confirmed the accuracy of the earlier results reported in [11] and [24]. Unlike in the former work, both analyses described in [24] and [26] assumed that the loading of the hemisphere took place in a rigid tensile testing machine. The two edges of the shell were taken to be clamped to rigid rings, with a fixed lower boundary, while the upper ring was moved vertically through a prescribed small distance. To get the vertical critical load those authors computed the meridional stresses at the equator. Bagchi [27] revisited the tensile instabilities of the truncated hemisphere in the context of finite-element techniques and simplified computational analyses based on initial geometric imperfections, while in [28] Shilkrut draws attention to the analogy between this buckling problem and pressurised caps/circular plates.

The investigation described in the following pages has been motivated in part by a recent paper [29] in which Yao's original work [11] was re-considered in the context of orthotropic and other more general shells of revolution. By invoking a so-called asymptotic simplification process of the relevant bifurcation equations, the authors of [29] were led to some extensions of the formulae proposed by

Bushnell [16]. Unfortunately, some of the claims made in [29] are incorrect and the simplification process employed therein does not seem to qualify as a true asymptotic approximation.

With this background, we start our investigation in the next section with a quick description of the mathematical formulation of the wrinkling problem studied by Yao [11], and this serves as the basis for the subsequent discussions. As with other similar problems for thin plates and shells, the bifurcation equations turn out to depend on a large parameter $\mu \propto (R/h) \gg 1$, where R is the radius of the hemisphere and h represents its thickness. In §3 the numerical solutions of these equations are illustrated for two different shell geometries and a sequence of increasing values for μ. We also use this as an opportunity to take a closer look at the aforementioned asymptotic approximation proposed recently ([29]) in connection to [11]. Guided in part by the numerical evidence, in §4 and §5 we then embark on the full asymptotic description of the eigenmodes and their associated eigenvalues (i.e., the critical loads). Further comparisons between the asymptotic results and the corresponding direct numerical simulations confirm the validity and usefulness of the new approximations derived herein. The paper concludes with a discussion of our key results and some remarks for possible extensions.

2 Outline of the wrinkling eigenproblem

We consider a truncated hemispherical thin shell of radius R and uniform thickness h ($0 < h/R \ll 1$) subjected to tensile axial forces proportional to $P > 0$. Following Yao's original work [11], it will be assumed that both edges of the shell are restrained from moving radially and from rotating; we refer to [17] or [30], which provide further details on the practical realisation of these constraints. In spherical polar coordinates, the geometry of the hemisphere can be described with the help of the two angles ϕ and θ that have the meaning indicated in Figure 2 (note that the definition of the former angle is slightly different from the one typically used in the literature; that would correspond to making the substitution $\phi \to \pi/2 - \phi$). In addition, the shell is assumed to be made of an isotropic elastic material characterised by the Young's modulus $E > 0$ and the Poisson's ratio $0 < \nu < 1/2$.

Bifurcations from a rotationally symmetric deformation of the truncated hemisphere can be easily obtained by employing the method of adjacent equilibrium in conjunction with a set of nonlinear differential equations that describes the behaviour of the shell. We use the Donnell-Mushtari-Vlasov (DMV) shallow shell theory (e.g., see [12, 13]). If the rotationally symmetric basic state corresponds to a transverse displacement $\mathring{w} \equiv \mathring{w}(\phi)$ and the membrane stresses $\mathring{N}_{\phi\phi} \equiv \mathring{N}_{\phi\phi}(\phi)$, $\mathring{N}_{\theta\theta} \equiv \mathring{N}_{\theta\theta}(\phi)$, it can then be shown that the linearised bifurcation equations can be cast in the form (see Appendix)

$$D\nabla_*^4 w - R\nabla_*^2\Phi - \underline{\mathcal{L}(\Phi)\mathring{w}_{,\phi\phi}} + \underline{\tan\phi\,\mathring{w}_{,\phi}\Phi_{,\phi\phi}} - R^2\big[\mathring{N}_{\phi\phi}w_{,\phi\phi} + \mathring{N}_{\theta\theta}\mathcal{L}(w)\big] = 0\,, \tag{2.1a}$$

$$\nabla_*^4\Phi + Eh\big[R\nabla_*^2 w + \underline{\mathcal{L}(w)\mathring{w}_{,\phi\phi}} - \underline{\tan\phi\,\mathring{w}_{,\phi}w_{,\phi\phi}}\big] = 0\,, \tag{2.1b}$$

where $D := Eh^3/12(1-\nu^2)$ is the usual bending rigidity of the shell, the subscripts preceded by a comma indicate (partial) differentiation with respect to the corresponding spherical polar coordinates, and

$$\nabla_*^2 \equiv \frac{\partial^2}{\partial\phi^2} - \tan\phi\,\frac{\partial}{\partial\phi} + \sec^2\phi\,\frac{\partial^2}{\partial\theta^2}\,, \qquad \nabla_*^4 \equiv \nabla_*^2\nabla_*^2\,, \tag{2.2a}$$

$$\mathcal{L} \equiv \sec^2\phi\,\frac{\partial^2}{\partial\theta^2} - \tan\phi\,\frac{\partial}{\partial\phi}\,. \tag{2.2b}$$

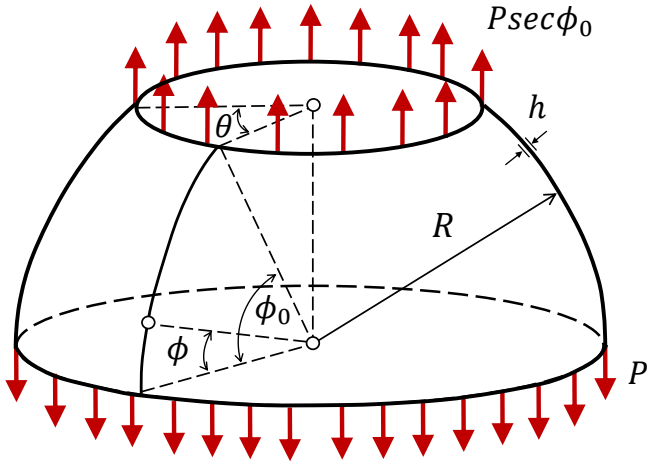

Figure 2: A truncated hemispherical shell subjected to vertical tensile loading uniformly distributed along the upper rim ($\phi = \phi_0$). Its geometry is described by the spherical polar coordinates $0 \leq \phi \leq \phi_0 \ll \pi/2$ and $0 \leq \theta < 2\pi$. The axial tensile load per unit circumferential length at the shell equator is $P > 0$.

In equations (2.1) the function $w \equiv w(\phi, \theta)$ represents an incremental (i.e., infinitesimal) transverse displacement, while $F \equiv F(\phi, \theta)$ corresponds to an Airy stress function that can be used to calculate the incremental membrane stresses in the buckled configuration according to the formulae

$$N_{\phi\phi} = \frac{1}{R^2}\big(\sec^2\phi\,\Phi_{,\theta\theta} - \tan\phi\,\Phi_{,\phi}\big)\,, \qquad N_{\theta\theta} = \frac{1}{R^2}\Phi_{,\phi\phi}\,, \tag{2.3a}$$

$$N_{\phi\theta} = \frac{1}{R^2}\big(\Phi_{,\phi\theta} + \tan\phi\,\Phi_{,\theta}\big)\sec\phi\,. \tag{2.3b}$$

To simplify matters the pre-buckling meridional rotation is set equal to zero, which amounts to discarding the underlined terms in (2.1). We also take the pre-buckling stress resultants $\mathring{N}_{\phi\phi}$ and $\mathring{N}_{\theta\theta}$ to be given by the linear membrane theory (see [14], p.27, for example), i.e.

$$\mathring{N}_{\phi\phi} = -\mathring{N}_{\theta\theta} = P\,\sec^2\phi\,. \tag{2.4}$$

As hinted in Figure 2, the vertical load applied to the shell is $P\sec\phi_0$ rather than P, so that the basic state assumes the form stated in (2.4). There is no loss of generality in doing this as, alternatively, one could simply re-scale the loading parameter to absorb the dependence on ϕ_0 (in order to ensure $\tan\phi$, $\sec\phi = \mathcal{O}(1)$ for $0 \leq \phi \leq \phi_0$, in what follows it will be tacitly assumed that $0 < \phi_0 \ll \pi/2$).

By introducing the non-dimensional quantities

$$\widehat{w} := \frac{w}{R}\,, \qquad \widehat{\Phi} := \frac{\Phi}{EhR^2}\,, \qquad \mu := \sqrt{12(1-\nu^2)}\left(\frac{R}{h}\right), \qquad \lambda := \frac{\mu^2 P}{Eh}\,, \tag{2.5}$$

and taking into account the aforementioned simplifications, the bifurcation system (2.1) reduces to

$$\nabla_*^4\widehat{w} - \mu^2\nabla_*^2\widehat{\Phi} - \lambda\big[\widehat{w}_{,\phi\phi} - \mathcal{L}(\widehat{w})\big]\sec^2\phi = 0\,, \tag{2.6a}$$

$$\nabla_*^4\widehat{\Phi} + \nabla_*^2\widehat{w} = 0\,, \tag{2.6b}$$

which (aside from some differences in notation) corresponds to the equations proposed by Yao in reference [11]. Unlike in that work, here we look for solutions with separable variables of (2.6) in the form

$$\widehat{w}(\phi,\theta) = W(\phi)\cos(m\theta)\,, \qquad \widehat{\Phi}(\phi,\theta) = F(\phi)\cos(m\theta)\,, \tag{2.7}$$

with the arbitrary integer $m \geq 0$ being determined subject to the requirement that it should render the global minimum of the curve $\lambda = \lambda(m)$. Performing the requisite calculations it turns out that the unknown amplitudes in (2.7) satisfy the linear system

$$\begin{bmatrix} \mathcal{L}_{11} & \mathcal{L}_{12} \\ \mathcal{L}_{21} & \mathcal{L}_{22} \end{bmatrix} \begin{bmatrix} W \\ F \end{bmatrix} = \begin{bmatrix} 0 \\ 0 \end{bmatrix}\,, \tag{2.8}$$

where

$$\mathcal{L}_{11} \equiv \frac{d^4}{d\phi^4} + \mathcal{A}_{113}\frac{d^3}{d\phi^3} + \mathcal{A}_{112}\frac{d^2}{d\phi^2} + \mathcal{A}_{111}\frac{d}{d\phi} + \mathcal{A}_{110}\,, \tag{2.9a}$$

$$\mathcal{L}_{12} \equiv \mathcal{A}_{122}\frac{d^2}{d\phi^2} + \mathcal{A}_{121}\frac{d}{d\phi} + \mathcal{A}_{120}\,, \tag{2.9b}$$

$$\mathcal{L}_{21} \equiv \mathcal{A}_{212}\frac{d^2}{d\phi^2} + \mathcal{A}_{211}\frac{d}{d\phi} + \mathcal{A}_{210}\,, \tag{2.9c}$$

$$\mathcal{L}_{22} \equiv \frac{d^4}{d\phi^4} + \mathcal{A}_{223}\frac{d^3}{d\phi^3} + \mathcal{A}_{222}\frac{d^2}{d\phi^2} + \mathcal{A}_{221}\frac{d}{d\phi} + \mathcal{A}_{220}\,, \tag{2.9d}$$

with the coefficients $\mathcal{A}_{ijk}$ being recorded below. In particular, for $\mathcal{L}_{11}$ and $\mathcal{L}_{12}$ we have

$$\begin{aligned}
&\mathcal{A}_{113} = -2\tan\phi\,,\\
&\mathcal{A}_{112} = -\left[2(1+m^2)+\lambda\right]\sec^2\phi + \tan^2\phi\,, && \mathcal{A}_{122} = -\mu^2\,,\\
&\mathcal{A}_{111} = -\left[(1+2m^2)+\lambda\right]\sec^2\phi\tan\phi\,, && \mathcal{A}_{121} = \mu^2\tan\phi\,,\\
&\mathcal{A}_{110} = m^2\sec^2\phi\left[(m^2-2-\lambda)\sec^2\phi - 2\tan^2\phi\right]\,, && \mathcal{A}_{120} = \mu^2 m^2\sec^2\phi\,,
\end{aligned}$$

while for $\mathcal{L}_{21}$ and $\mathcal{L}_{22}$,

$$\begin{aligned}
&\mathcal{A}_{223} = -2\tan\phi\,,\\
&\mathcal{A}_{222} = -2(1+m^2)\sec^2\phi + \tan^2\phi\,, && \mathcal{A}_{212} = 1\,,\\
&\mathcal{A}_{221} = -(1+2m^2)\sec^2\phi\tan\phi\,, && \mathcal{A}_{211} = -\tan\phi\,,\\
&\mathcal{A}_{220} = m^2\sec^2\phi\left[(m^2-2)\sec^2\phi - 2\tan^2\phi\right]\,, && \mathcal{A}_{210} = -m^2\sec^2\phi\,.
\end{aligned}$$

The equations (2.8) are to be solved subject to the following boundary conditions (see [11])

$$W = \frac{dW}{d\phi} = 0\,, \qquad \text{for } \phi = 0, \phi_0\,, \tag{2.10a}$$

$$F = \frac{dF}{d\phi} = 0\,, \qquad \text{for } \phi = 0, \phi_0\,. \tag{2.10b}$$

This completes the description of the equations that form the starting point for the subsequent developments. The boundary-value problem consisting of (2.8) and (2.10) provides and alternative formulation to the simple-minded Galerkin strategy adopted by Yao [11]. The angle ϕ_0 is assumed to be given, while $\lambda \equiv \lambda(m;\mu)$ represents the unknown eigenvalue. It is further noted that $m \in \mathbb{N}$ is also unknown at this stage and, for each fixed ϕ_0, this parameter will have to be determined so that it renders the global minimum of the curve λ versus m (which would roughly correspond to a minimum-energy configuration reached by the deformed shell). To this end, as it is customary in problems of this type, the mode number will be regarded as a positive continuous parameter, i.e. $m \in \mathbb{R}_+$; the *critical eigenvalue*, λ_c, and the *critical mode number*, m_c, are thus defined by the requirements

$$\lambda_c = \min_{m>0} \lambda(m;\mu)\,, \qquad \text{with} \quad \lambda_c = \lambda(m_c;\mu)\,. \tag{2.11}$$

In order to glean further insight into the structure that underpins the bifurcation equations (2.8) subject to (2.10), we turn to some direct numerical simulations of those equations. All numerical results reported in the next section are obtained by using standard numerical routines in MATLAB.

3 Numerical simulations

Since the geometry of interest is hemispherical, the re-scaled configuration is fully determined by the choice of the *altitude angle* ϕ_0 (which defines the location of the upper rim). Taken at face value, the use of the linear membrane pre-buckling state in the model described in the previous section would seem to impose some severe restrictions on what that angle might be. However, numerical evidence reported by previous investigators (e.g., see [16, 17, 24]) suggests otherwise. For example, according to [29] earlier numerical solutions based on using the DMV bifurcation equations and taking into account the bending of the basic state showed very little difference from Yao's [11] previous results, provided that $\phi_0 > 10\mu^{-1/2} \equiv \phi_I$. Further numerical evidence presented by Bushnell [16, 17] also indicates that the limit of applicability of the linear membrane basic state would be satisfied for angles ϕ_0 for which $\phi_0 < \pi/2 - 20\mu^{-1/2} \equiv \phi_{II}$ (cf. [29]). In [16] it is also reported that for very shallow shells (i.e., very small ϕ_0) the nonlinear bending pre-buckling solution yielded critical loads different from those predicted by the linear momentless basic state. We have carried out extensive numerical simulations for $10^\circ \le \phi_0 \le 60^\circ$, but in the interest of brevity we shall include here only a small representative sample of results. For the same reason we have fixed the Poisson's ratio to $\nu = 0.3$ in all of our subsequent examples.

In Figure 3 we illustrate the form of the response curves $\lambda(m)$ for eight values of (R/h) equally spaced between 5×10^2 an 19×10^2 (recall from (2.5) that $\mu \propto (R/h)$). The form of the curves shown was derived by solving the bifurcation system (2.8)-(2.10) for λ, given a fixed μ and $\phi_0 = 23^\circ\, 30'$. For each μ the corresponding curve rises as both $m \to 0^+$ and $m \to +\infty$, with the minimum $\lambda = \lambda_c$ occurring at $m = m_c$. In order to simplify the presentation somewhat the various curves are shown only for $m < m_c$, and the dashed line depicts the locus of the critical points as μ varies. It is clear that both λ_c and m_c increase with (R/h), although the former feature is partly an artefact of the scaling choice adopted in (2.5). A closer look at these numerical results would seem to suggest that $\lambda_c = \mathcal{O}(\mu)$ and $m_c = \mathcal{O}(\mu^{1/2})$, an observation that will be fully explored in due course.

Examples of critical eigenmodes of the original problem are shown in Figure 4 for the same sequence of (R/h)-values as indicated above, but this time we use two different shell geometries. Only the incremental transverse displacements are included in our plots because the corresponding F-functions

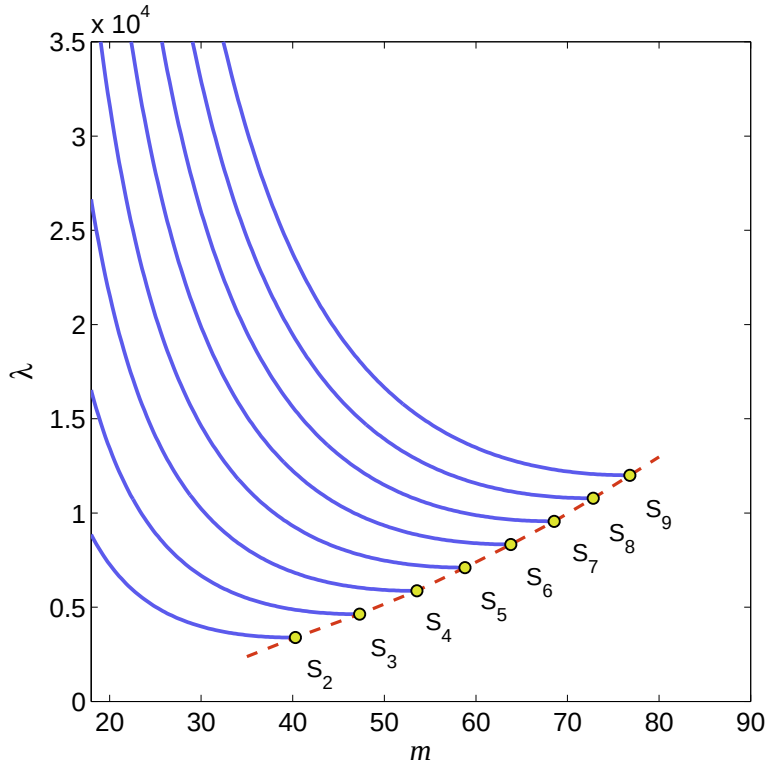

Figure 3: Dependence of the non-dimensional load λ on the mode number m for an increasing set of eight values of (R/h) and $\phi_0 = 23^\circ\, 30'$. The points $S_j \equiv (\lambda_c, m_c)$, where $(R/h) = (2j+1) \times 10^2$ and $j = 2, 3, \ldots, 9$, represent the minima of the respective curves and identify the corresponding critical values. Only those parts of the curves with $m < m_c$ are shown; the Poisson's ratio $\nu = 0.3$.

turn out to be (approximately) just scaled versions of their W-counterparts; as we shall see shortly this is not merely a coincidence. In both windows the eigenmodes appear to shift towards the upper rim of the truncated hemisphere as (R/h) grows. For the smaller value of $\phi_0 \simeq 0.4$ (rad) used in the left window this phenomenon is relatively weak. The reason behind this behaviour admits a simple explanation; since the differential equations are integrated over $[0, \phi_0]$, it should be clear that the largeness of μ will be offset by the meridional angle associated with the right end of the integration range. On the other hand, when $\phi_0 \simeq 0.6$ (rad), i.e. the situation depicted in the right window of Figure 4, the localisation tendency of the eigenmodes becomes more pronounced (we are using the same (R/h)-values in both windows). These observations open up the possibility that in the large-μ limit the solutions of the eigenproblem (2.8)-(2.10) might be of the boundary-layer type. If this is true, then the original governing equations ought to admit some rational simplifications that could potentially be exploited to capture the dependence of the critical load (λ_c) and mode number (m_c) on the asymptotic parameter $\mu \propto (R/h)$. Even though this simplified approach would strictly speaking be valid only for $\mu \gg 1$, experience shows that such asymptotic formulae can be expected to approximate exact values well, even for moderate or low values of the perturbation parameter (e.g., see [1, 31, 32]).

In reference [29] an attempt was made to provide an approximation for the critical load λ_c in terms of known quantities. While the final result presented by those authors performs (more or less) well, some of the mathematical methods by which it was derived are unorthodox, as we now explain.

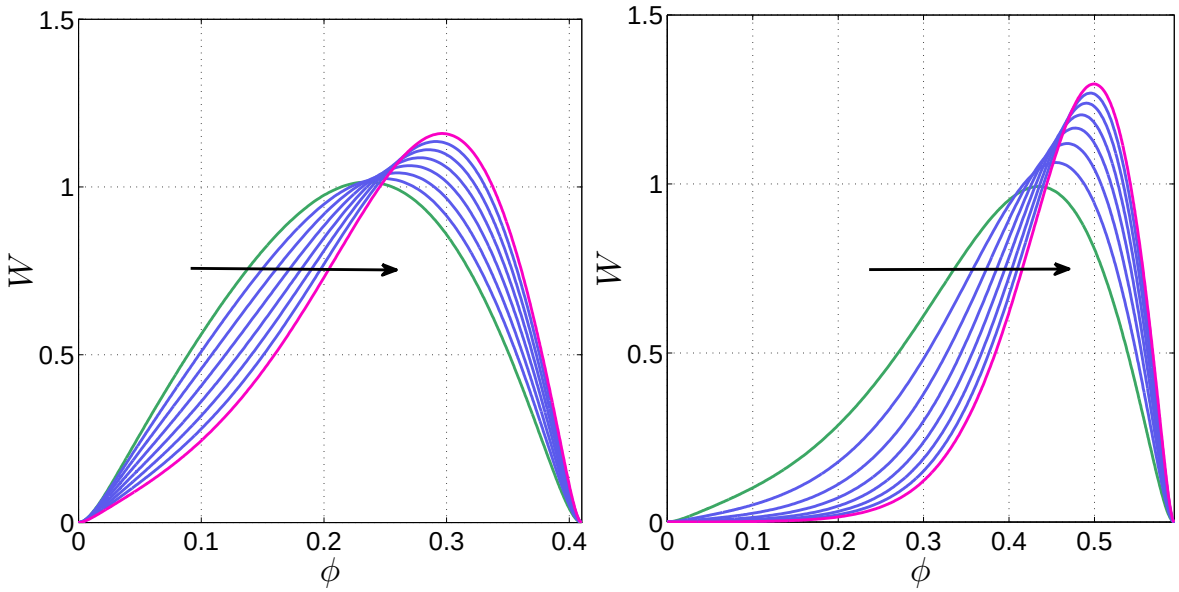

Figure 4: Sequences of *critical eigenmodes* corresponding to the same values of (R/h) as in Fig. 3, and for two different geometries: $\phi_0 = 23^\circ\,30'$ (left) and $\phi_0 = 34^\circ$ (right). The arrows indicate the direction in which $\mu \propto (R/h)$ increases, while the first and last eigenmodes in each sequence are coloured differently; these are shown as green and red-pink, respectively. All solutions are normalised so that $\int_0^{\phi_0} W^2(\phi)\,\mathrm{d}\phi = 0.2$ and the Poisson's ratio $\nu = 0.3$ in both windows.

Kalamkarov and Andrianov [29] implicitly assumed in their analysis that both $\widehat{w}(\phi,\theta)$ and $\widehat{\Psi}(\phi,\theta)$ in (2.6) consist of a slowly varying part, extending over an $\mathcal{O}(1)$ region of the shell's lateral surface, plus an edge effect. Clearly, such an assumption is at odds with the numerical evidence included in Figure 4. Assuming further that buckling occurs with the formation of a large number of half-waves in the azimuthal direction, they formally reduced the bifurcation equations (2.6) to a single PDE,

$$\frac{\partial^4 \widehat{w}}{\partial\theta^4} + \lambda\frac{\partial^2 \widehat{w}}{\partial\theta^2} + \mu^2\cos^4\phi\,\widehat{w} = 0\,. \tag{3.1}$$

The presence of the rogue term '$\cos^4\phi$' is problematic and already casts doubt on the usefulness of the simplified equation obtained. As a remedy, the authors decided to invoke the method of "freezing coefficients" (e.g., [33]). To this end, it was argued that ϕ in the above equation could be replaced by some fixed value, $\phi = \phi_*$ (say), where $\mathring{N}_{\theta\theta} \equiv \mathring{N}_{\theta\theta}(\phi)$ has a maximum. This could be a sensible assumption, although we have shown in a recent study [34] that in a thin elastic shell there is a subtle interplay between the geometric and mechanical rigidity, on the one hand, and the localisation of buckling patterns, on the other. Ignoring such fine details for the moment, this assumption raises a dilemma since for the case of the membrane basic state (used in their work) such maximum would correspond to $\phi_* \equiv \phi_0$. To circumvent the difficulty, the authors of [29] propose the *empirical* value $\phi_* := \phi_0 - 2^{5/2}K\mu^{-1/2}$ in which $K := \big[3(1-\nu^2)\big]^{1/4}$. The rationale behind this choice is apparently linked to the usual $\mathcal{O}(\mu^{-1/2})$ bending layer associated with clamped boundary conditions (i.e., the aforementioned edge effect). This is not a plausible argument because, as we are going to see shortly, the maximum transverse displacement occurs inside a much bigger boundary layer. In the case of a *nonlinear* basic state Bushnell [16] found that $|\mathring{N}_{\theta\theta}|$ does have a local maximum in the close proximity of the edge $\phi = \phi_0$, and he also noticed that the maximum transverse eigendeformation takes place

around the same location. But these observations were made in the context of a rather different (more refined) set of bifurcation equations, which only confuses the matter at hand even more.

Expressed in the notation of this paper, formula (10) from [29] can be re-arranged to become

$$\lambda_c = 2\mu\cos^2(\phi_0 - 2^{5/2}K\mu^{-1/2})\,, \tag{3.2}$$

and in the limit $\mu \gg 1$ one can write

$$\lambda_c = \sum_{j=0}^{\infty} \Lambda_j(\phi_0)\mu^{1-j/2}\,, \tag{3.3}$$

where the shorthand notations $\Lambda_j \equiv \Lambda_j(\phi_0)$ for $j = 0, 1, 2, \ldots$ correspond to

$$\Lambda_0 := 2\cos^2\phi_0\,, \qquad \Lambda_1 := 2^{7/2}K\sin(2\phi_0)\,, \qquad \Lambda_2 := -2^6K^2\cos(2\phi_0)\,,$$

$$\Lambda_3 := -\frac{2^{19/2}}{3}K^3\sin(2\phi_0)\,, \qquad \Lambda_4 := \frac{2^{11}}{3}K^4\cos(2\phi_0)\,, \qquad \Lambda_5 := \frac{2^{29/2}}{15}K^5\sin(2\phi_0)\,, \quad \text{etc}\,.$$

The accuracy of the predictions generated by the full formula (3.2) is illustrated in Figure 5 by plotting the corresponding relative errors (*R.E.*) for the two values of ϕ_0 used in Figure 4. The four-term approximation that transpires from (3.3) is also included – note that by keeping this particular number of terms the theoretical truncation error is expected to be $\mathcal{O}(\mu^{-1})$. In both cases the truncated

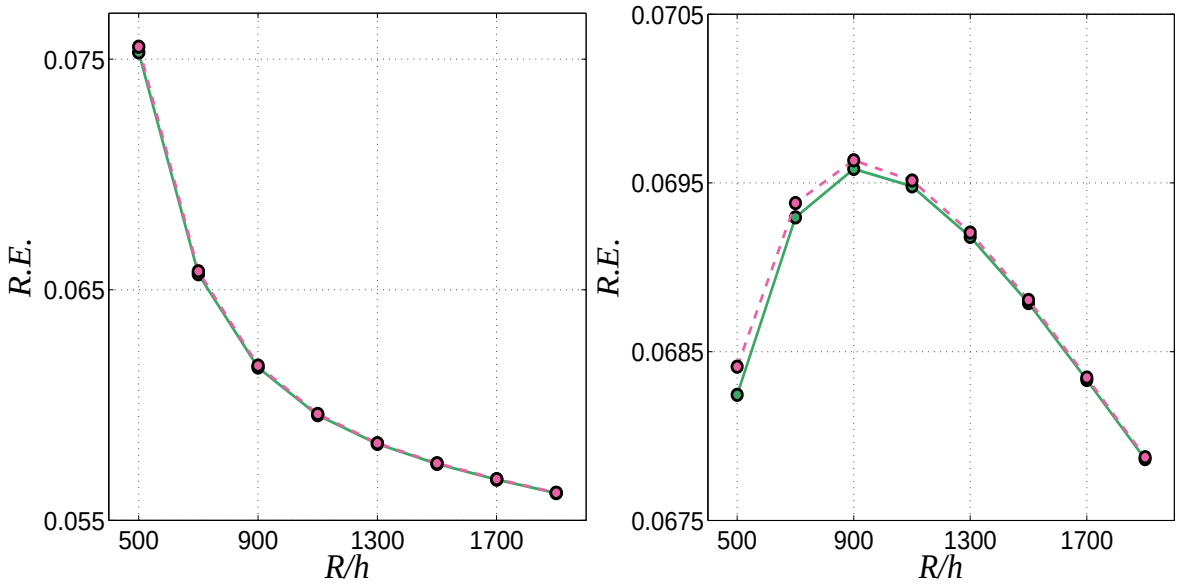

Figure 5: Relative errors (*R.E.*) for the formula (3.2) and the four-term $\mathcal{O}(\mu^{-1})$ truncation obtained from (3.3). On the left, $\phi_0 = 23^\circ\,30'$, while the other window shows the comparison for $\phi_0 = 34^\circ$. The markers and the lines in green correspond to the full result; the pink is used for the truncated series.

series mirrors faithfully the full-form predictions (3.2), and the relative errors in both windows are relatively reasonable as engineering approximations; these errors range between approximately 5.5% and 7.5%. Of particular concern is the *R.E.* for $\phi_0 = 34^\circ$ (right window), which appears to display some peculiar behaviour (a local maximum). This is likely to be an immediate consequence of the

limited range of validity for the choice of the angle ϕ_*. Later in this study we are going to return to the approximation (3.2) in order to show how one can improve it. This requires a more detailed understanding of the edge effect and its possible interaction with other boundary-layer type solutions that the bifurcation system (2.8)-(2.10) can accommodate in the limit $\mu \gg 1$. The next two sections provide the relevant details of such an analysis.

4 Asymptotic approximations

From the discussion of the previous section we anticipate that the critical modes of the boundary-value problem consisting of (2.8) and (2.10) are confined to a relatively large layer attached to the rim $\phi = \phi_0$ of the truncated hemisphere. To find the relevant scalings we start by noting that if we consider (2.8) in a boundary layer $\phi = \phi_0 - \mathcal{O}(\delta)$ with $\mu^{-1/2} \ll \delta \ll 1$ then a distinguished limit of the bifurcation system can be obtained from the balances $\mathcal{A}_{110}W \sim \mathcal{A}_{120}F$ and $\mathcal{A}_{210}W \sim \mathcal{A}_{220}F$ (since all the derivative terms turn out to be smaller than these). Assuming that $W = \mathcal{O}(\mu^{t_1})$ and $F = \mathcal{O}(\mu^{t_2})$ for some $t_1,\, t_2 \in \mathbb{R}$, the balancing of the terms mentioned above gives $\mu^{t_1} m^4 \sim \mu^{t_1} m^2 \lambda \sim \mu^{t_2+2} m^2$ and $\mu^{t_1} m^2 \sim \mu^{t_2} m^4$, whereby $m^2 \sim \lambda$, $\lambda \sim \mu^{t_2-t_1+2}$, $m^2 \sim \mu^{t_1-t_2}$ and hence $t_2 = t_1 - 1$. The linearity of our equations ensures that we can set $t_1 = 0$ and it remains that $t_2 = -1$. Note that with this information in hand we then have $m^2 \sim \mu$ and $\lambda \sim \mu$. To fix the size of the boundary layer we have to ensure that our reduced equations have some spatially varying terms. Expanding $(\sec\phi)^4$ in Taylor series suggests that we might get such a term from a balance of $\mathcal{A}_{112}W''$ and $\mathcal{A}_{110}W$ (at the next order), which would require $m^4\delta \sim \delta^{-2}m^2$ whence $\delta \sim \mu^{-1/3}$. These elementary calculations set the stage for the next key development.

Motivated by the above discussion we introduce the stretched coordinate Y defined by

$$\phi = \phi_0 - \mu^{-1/3} Y\,, \qquad Y = \mathcal{O}(1)\,, \tag{4.1}$$

and set $m^2 = \mu M_0$ for some $M_0 = \mathcal{O}(1)$ (that is yet to be determined). We look for solutions of (2.8) with an ansatz of the form

$$\lambda = \lambda_0\mu + \lambda_1\mu^{2/3} + \lambda_2\mu^{1/2} + \lambda_3\mu^{1/3} + \dots\,, \tag{4.2a}$$

$$\boldsymbol{u} = \boldsymbol{u}^{(0)}(Y) + \mu^{-1/6}\boldsymbol{u}^{(1)}(Y) + \mu^{-1/3}\boldsymbol{u}^{(2)}(Y) + \mu^{-1/2}\boldsymbol{u}^{(3)}(Y) + \mu^{-2/3}\boldsymbol{u}^{(4)}(Y) + \dots\,, \tag{4.2b}$$

where

$$\boldsymbol{u} := \begin{bmatrix} W \\ \\ \mu F \end{bmatrix}\,, \qquad \boldsymbol{u}^{(j)} := \begin{bmatrix} W_j \\ \\ F_j \end{bmatrix}\,, \qquad (j = 0, 1, 2, \dots)\,.$$

The constants $\lambda_j = \mathcal{O}(1)$ in (4.2a) and the individual terms $\boldsymbol{u}^{(j)}$ on the right-hand side of (4.2b) are found as usual by substituting the assumed form of the solution in the original differential equations, collecting like powers of μ, and setting to zero the corresponding coefficients. The outcome is a hierarchy of equations that can be cast in the form

$$\boldsymbol{A}\boldsymbol{u}^{(j)} = \boldsymbol{b}^{(j)}\,, \qquad (j = 0, 1, 2, \dots)\,, \tag{4.3}$$

with

$$\boldsymbol{A} := \begin{bmatrix} (M_0 - \lambda_0)\sec^2\phi_0 & 1 \\ \\ -1 & M_0\sec^2\phi_0 \end{bmatrix} \qquad \text{and} \qquad \boldsymbol{b}^{(j)} := \begin{bmatrix} \mathcal{R}_{j1} \\ \\ \mathcal{R}_{j2} \end{bmatrix}\,;$$

the expressions for the components of the vectors $\boldsymbol{b}^{(j)}$ will be recorded below as we go along.

With this information into the zeroth-order equations we find $\mathcal{R}_{01} = \mathcal{R}_{02} \equiv 0$, so we have a homogeneous linear system. Its consistency requires that $\det(\boldsymbol{A}) = 0$, whence

$$\lambda_0 = M_0 + \frac{\cos^4\phi_0}{M_0}\,. \tag{4.4}$$

Minimising λ_0 with respect to M_0 gives immediately

$$\lambda_0 = 2\cos^2\phi_0 \qquad \text{and} \qquad M_0 = \cos^2\phi_0\,. \tag{4.5}$$

From the leading-order equations it also transpires that $W_0 = F_0$, and the function $W_0 \equiv W_0(Y)$ remains arbitrary at this stage.

The right-hand side of (4.3) for the first-order equations is identically zero, so we are left with $W_1 = F_1$. Again, the function $W_1 \equiv W_1(Y)$ is arbitrary and will have to be identified by exploring the higher-order equations that follow from (4.3).

The first significant piece of information emerges at the second order, where

$$\mathcal{R}_{21} := -2Y\tan\phi_0 W_0 + \lambda_1\sec^2\phi_0 W_0 + 5W_0''\,, \tag{4.6a}$$

$$\mathcal{R}_{22} := 2Y\tan\phi_0 + W_0''\,, \tag{4.6b}$$

and the 'dash' stands for differentiation with respect to Y. The consistency of the second-order problem requires $\mathcal{R}_{21} - \mathcal{R}_{22} = 0$, which leads to a scaled Airy-type equation

$$W_0'' - (\Gamma_1 Y + \Gamma_2)W_0 = 0\,, \tag{4.7}$$

with

$$\Gamma_1 := \tan\phi_0 \qquad \text{and} \qquad \Gamma_2 := -\frac{1}{4}\lambda_1\sec^2\phi_0\,. \tag{4.8}$$

Equation (4.7) can be transformed into standard form by putting $Z := \Gamma_1^{-2/3}(\Gamma_1 Y + \Gamma_2)$ whereupon it follows that $d^2\widehat{W}_0/dZ^2 - Z\widehat{W}_0 = 0$, with $\widehat{W}(Z) \equiv W_0(Y)$. The solution of relevance to the present context is $\widehat{W}_0 = Ai(Z)$, where 'Ai' is the Airy function that decays exponentially quickly as $Z \to +\infty$.

The boundary conditions (2.10) at $\phi = \phi_0$ (i.e., $Y = 0$) cannot both be imposed at this juncture – this suggests that the main $Y = \mathcal{O}(1)$ region will be supplemented by an inner zone, but we should ensure that $W_0 \to 0$ as $Y \to 0^+$. We recall in passing that, in addition to exponentially decaying as $Z \to +\infty$, the Airy function has a countable set of zeros along the negative Z-axis; the first occurs at $(-\zeta_0) \simeq -2.338$, so we make certain that $W_0(Y) = 0$ at $Y = 0$ by demanding $\Gamma_1^{-2/3}\Gamma_2 = -\zeta_0$. If the expressions (4.8) are substituted in this relation, it follows immediately that

$$\lambda_1 = 4\zeta_0\cos^2\phi_0\tan^{2/3}\phi_0\,. \tag{4.9}$$

The λ_2-term in (4.2a) comes into play at the third order; the right-hand side of (4.3) has components

$$\mathcal{R}_{31} := -2Y\tan\phi_0 W_1 + \lambda_1\sec^2\phi_0 W_1 + \lambda_2\sec^2\phi_0 W_0 + 5W_1''\,, \tag{4.10a}$$

$$\mathcal{R}_{32} := 2Y\tan\phi_0 + W_1''\,, \tag{4.10b}$$

and imposing the solvability condition $\mathcal{R}_{31} - \mathcal{R}_{32} = 0$ gives the inhomogeneous equation

$$W_1'' - (\Gamma_1 Y + \Gamma_2)W_1 = -\frac{1}{4}\lambda_2\sec^2\phi_0 W_0(Y)\,, \tag{4.11}$$

which admits the particular solution

$$\widehat{W}_1(Z) = -\frac{\lambda_2 \sec^2\phi_0}{4\tan^{2/3}\phi_0}\, Ai'(Z)\,, \tag{4.12}$$

with $\widehat{W}_1(Z) = W_1(Y)$ and the 'dash' denotes differentiation with respect to Z. While for the time being λ_2 remains arbitrary, it will be shown in the next section that its expression is fixed by matching the asymptotic expansion (4.2b) with the usual bending layer at the upper rim ($\phi = \phi_0$).

To check the matching of the current solution with the aforementioned bending layer we go one step further and calculate the governing equations for W_4 and F_4. As the procedure should now be clear, we shall be content to simply mention that the consistency condition $\mathcal{R}_{41} - \mathcal{R}_{42} = 0$ yields an inhomogeneous Airy-like equation; after considerable manipulations, expressed in terms of the Z-variable, this equation can be stated as

$$\frac{d^2\widehat{W}_2}{dZ^2} - Z\widehat{W}_2 = (B_{00} + B_{01}Z + B_{02}Z^2)Ai(Z) + B_{10}Ai'(Z) + (B_{20} + B_{21}Z)Ai^{(2)} + B_{40}Ai^{(4)}(Z)\,, \tag{4.13}$$

where

$$B_{00} := -\frac{\lambda_3 \sec^2\phi_0}{4\tan^{2/3}\phi_0} + \frac{(3\tan^2\phi_0 - 1)\zeta_0^2}{2\tan^{4/3}\phi_0}\,,$$

$$B_{01} := -\frac{\zeta_0 \sec^2\phi_0}{\tan^{4/3}\phi_0}\,, \quad B_{02} := -\frac{1 + 5\tan^2\phi_0}{2\tan^{4/3}\phi_0}\,, \quad B_{10} := \tan^{2/3}\phi_0 - \frac{\lambda_2 \sec^2\phi_0}{4\tan^{2/3}\phi_0}\,,$$

$$B_{20} := \zeta_0 \tan^{2/3}\phi_0\,, \quad B_{21} := 2\tan^{2/3}\phi_0\,, \quad B_{40} := \frac{1}{4}\tan^{2/3}\phi_0\,.$$

It is relatively straightforward to identify a particular integral for (4.13), and we refer the reader to our past work (e.g., [35, 36]) for details of similar examples. Here, we record only the final result

$$W_2 = \frac{1}{5}(B_{02} + B_{21} + B_{40})Ai^{(5)}(Z) + \frac{1}{3}(B_{01} + B_{20})Ai^{(3)}(Z) + \frac{1}{2}\big[B_{10} - 2(B_{21} + B_{02})\big]Ai^{(2)}(Z) + B_{00}Ai'(Z)\,, \tag{4.14}$$

and for further reference we note that

$$W_2\big|_{Y=0} = \left[\frac{1}{5}(B_{02} + B_{21} + B_{40})\zeta_0^2 + \frac{1}{3}(B_{01} + B_{20})\zeta_0 + B_{00}\right] Ai_0'\,, \tag{4.15}$$

with $Ai_0' \equiv Ai'(\zeta_0)$.

The coefficient B_{00} introduced above depends on λ_3, while the definition of B_{10} contains λ_2. Both λ-terms will be identified by supplementing the present analysis with additional information regarding the behaviour of $W_1(Y)$ and $W_2(Y)$ as $Y \to 0^+$.

5 The bending layer & matching

It was noted in the previous section that, while we could make W_0 vanish on $Y = 0$, we could not satisfy the derivative condition part of (2.10a). This can be resolved within a thin bending layer of size $\mathcal{O}(\mu^{-1/2})$. This motivates the introduction of a new re-scaled coordinate X such that

$$\phi = \phi_0 - \mu^{-1/2} X\,, \qquad X = \mathcal{O}(1)\,. \tag{5.1}$$

In the bending layer the transverse displacement and the stress function amplitudes in (2.8) are expanded according to

$$W = \mu^{-1/6} g_0(X) + \mu^{-1/3} g_1(X) + \mu^{-1/2} g_2(X) + \dots\,, \tag{5.2a}$$

$$F = \mu^{-7/6} f_0(X) + \mu^{-4/3} f_1(X) + \mu^{-3/2} f_2(X) + \dots\,, \tag{5.2b}$$

where g_j, f_j $(j = 0, 1, 2, \dots)$ will be determined sequentially as briefly explained next.

To this end we note that the boundary conditions at the upper rim of our shell – see (2.10), will assume the form

$$g_j = f_j = \frac{dg_j}{dX} = \frac{df_j}{dX} = 0\,, \qquad \text{for} \quad X = 0\,, \qquad (j = 0, 1, 2, \dots)\,, \tag{5.3}$$

and the coefficients of our boundary-layer ansatz will also be subject to the usual decay conditions

$$g_j,\ f_j,\ \frac{dg_j}{dX},\ \frac{df_j}{dX} \to 0 \qquad \text{as} \quad X \to +\infty\,, \qquad (j = 0, 1, 2, \dots)\,. \tag{5.4}$$

Standard calculations reveal that the leading-order approximation corresponding to (5.2) satisfies the differential system

$$\begin{bmatrix} D^4 - 4D^2 - 1 & -D^2 + 1 \\ D^2 - 1 & D^4 - 2D^2 + 1 \end{bmatrix} \begin{bmatrix} g_0(X) \\ f_0(X) \end{bmatrix} = \begin{bmatrix} 0 \\ 0 \end{bmatrix}\,, \qquad D \equiv d/dX\,. \tag{5.5}$$

Since this is a constant-coefficient problem we look for solutions in the form $g_0 = \widehat{g}_0 \exp(pX)$ and $f_0 = \widehat{f}_0 \exp(pX)$, where the numbers p, $\widehat{g}_0$ and $\widehat{f}_0$ are yet to be found. The characteristic equation satisfied by p turns out to be $p^2(p^2-1)^2(p^2-4) = 0$, and hence the solutions of (5.5) will be linear combinations of real exponentials (as normally expected).

Without going into the routine details of identifying the solutions consistent with (5.3) and (5.4), we eventually find

$$g_0(X) = \gamma_0\big(1 - 4X - 3\mathrm{e}^{-2X} + 2\mathrm{e}^{-X}\big)\,, \qquad f_0(X) = \gamma_0\left[1 - 4X + \mathrm{e}^{-2X} - 2(1-2X)\mathrm{e}^{-X}\right]\,, \tag{5.6}$$

where $\gamma_0 \in \mathbb{R}$ is arbitrary. Matching (4.2b) and (5.2a) at leading order yields $\gamma_0 = -\tan^{1/3}\phi_0 Ai_0'/4$ and

$$\lambda_2 = \tan\phi_0 \cos^2\phi_0\,. \tag{5.7}$$

It turns out that f_1 and g_1 satisfy the same equation (5.5), and hence the corresponding functions will have the same form as in (5.6), but with a (possibly) different constant of proportionality, $\gamma_1 \in \mathbb{R}$ (say). Then, matching (4.2b) and (5.2a) at the next order produces again $\gamma_1 = -\tan^{1/3}\phi_0 \mathrm{Ai}_0'/4$,

whence we discover that $W_2\big|_{Y=0} = \gamma_1$. In conjunction with the result (4.15) derived in the previous section, this leads eventually to an expression for λ_3 in (4.2a),

$$\lambda_3 = \tan\phi_0 \cos^2\phi_0 \left[1 + \frac{(87\tan^2\phi_0 - 56)\zeta_0^2}{15\tan^{5/3}\phi_0}\right], \tag{5.8}$$

where use has been made of (5.7).

We can now state the final form of our approximation. On substituting (4.5), (4.9), (5.7) and (5.8) into (4.2a), it follows that the critical load can be represented as

$$\lambda_c \sec^2\phi_0 = 2\mu + 4\zeta_0 \tan^{2/3}\phi_0\, \mu^{2/3} + \tan\phi_0\, \mu^{1/2} + \tan\phi_0 \left[1 + \frac{(87\tan^2\phi_0 - 56)\zeta_0^2}{15\tan^{5/3}\phi_0}\right] \mu^{1/3} + \ldots \tag{5.9}$$

or, in terms of the actual physical variables,

$$\begin{aligned} \frac{P_c \sec^2\phi_0}{Eh} = {} & \alpha_1(1-\nu^2)^{-1/2}\left(\frac{h}{R}\right) + \alpha_2(1-\nu^2)^{-2/3}\tan^{2/3}\phi_0 \left(\frac{h}{R}\right)^{4/3} \\ & + \alpha_3(1-\nu^2)^{-3/4}\tan\phi_0 \left(\frac{h}{R}\right)^{3/2} \\ & + \alpha_4(1-\nu^2)^{-5/6}\tan\phi_0 \left[1 + \frac{(87\tan^2\phi_0 - 56)\zeta_0^2}{15\tan^{5/3}\phi_0}\right] \left(\frac{h}{R}\right)^{5/3} + \ldots, \end{aligned} \tag{5.10}$$

where

$$\alpha_1 \simeq 0.57735\,, \qquad \alpha_2 \simeq 1.78422\,, \qquad \alpha_3 \simeq 0.15501\,, \qquad \alpha_4 \simeq 0.12609\,.$$

The accuracy of our main result (5.9) is illustrated in Figure 6. In the left window we show the dependence of $\mu^{-2}\lambda_c \sec\phi_0$ on (R/h) for the same two values of ϕ_0 that were considered earlier in Figure 4. The continuous blue lines are obtained by solving (2.8)-(2.10) for $(R/h) = (5+j)\times 10^2$, with $j = 0, 1, 2, \ldots, 14$; the (orange) dashed line together with the triangular markers represent the formula (5.9) for $\phi_0 = 34^\circ$, while the (green) round markers and the dashed line are their counterpart for $\phi_0 = 23^\circ\, 30'$. The relative errors (*R.E.*) between the asymptotic and numerical results included in the right window confirm that the accuracy in the former case increases as the eigenmodes become more localised. In particular, for the larger ϕ_0-angle *R.E.* $\simeq 1.7\%$ for $(R/h) = 5\times 10^2$, and this value drops below 1% for (R/h) greater than 16×10^2. The relative errors for the smaller angle are somewhat larger, with *R.E.* $\simeq 6.2\%$ for $(R/h) = 5\times 10^2$, although this error reduces to 2.4% for $(R/h) = 17\times 10^2$. The origin of this feature can be traced back to the shape of the eigenmodes displayed in left window of Figure 4; as the entire asymptotic work was carried out under the assumption that the eigenmodes were localised near $\phi = \phi_0$, it is not at all surprising that we encounter some loss of accuracy in that case. We mention in passing that the one-term approximation for the critical mode number, $m_c = \mu^{1/2}\cos\phi_0 + \ldots$, exhibits similar relative errors (ranging between approximately 3.5% and 6%), but in the interest of brevity we leave out detailed comparisons.

6 Discussion & final remarks

We have re-visited the tensile buckling of a truncated thin elastic hemisphere subjected to pulling vertical forces uniformly distributed along its upper rim. Our primary interest has been in exploring

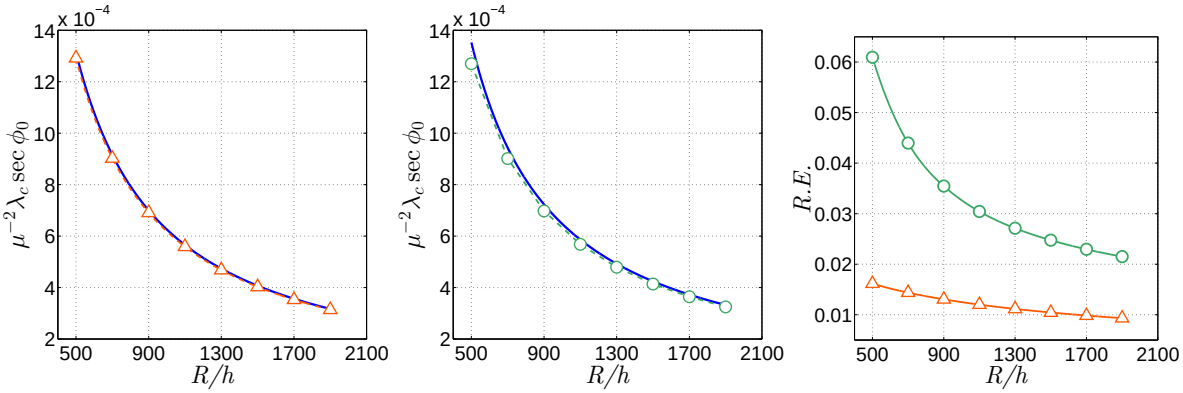

Figure 6: Comparisons between the asymptotic prediction (5.9) and direct numerical simulations of the bifurcation equation (2.8) subject to the boundary conditions (2.10); the Poisson's ratio $\nu = 0.3$. In the first two windows (from left to right) the numerical data is shown with the continuous line, while the triangular and round markers represent the asymptotic predictions for $\phi_0 = 34^\circ$ (first window) and $\phi_0 = 23^\circ\, 30'$ (second window). The corresponding relative errors ($R.E.$) are illustrated in the rightmost window (where the same type of markers are used to identify the results for each set of data).

and understanding the asymptotic structure of the corresponding DMV system of bifurcation equations (2.6), an aspect that does not seem to have received much attention so far. By focusing on the large-μ regime, where $\mu \propto (R/h)$, we have shown that, under certain conditions, the buckling phenomenon considered in this paper can be described by a familiar Airy-type layer already encountered in our previous works on the wrinkling of thin elastic plates in tension (e.g., [2, 36, 37]). However, unlike in those studies, the new Airy-type layer has a much larger spatial extent, occupying an $\mathcal{O}(\mu^{-1/3})$ region adjacent to the upper rim of the truncated shell. The presence of a nested $\mathcal{O}(\mu^{-1/2})$ bending layer made it possible to resolve the asymptotic structure of the corresponding eigendeformations, and led us to an accurate four-term asymptotic estimate for the critical loads. We remark in passing that the slow localisation tendency of the eigenmodes recorded in Figure 4 is also related to the fact that the "small" parameter in the bifurcation equations is $\mu^{-1/6}$ rather than μ^{-1}.

The terms in our asymptotic expansion (5.9) depend on the altitude angle ϕ_0 that defines the geometry of the truncated hemisphere. The asymptotic results corresponding to (4.2) will cease to provide a reasonably accurate approximation for the solution of the bifurcation problem (2.8)-(2.10) if some of the adjacent terms in (4.2a) become comparable. For example, the first two terms in (5.9) will have the same order of magnitude if $\phi_0 \sim \pi/2 - (2\zeta_0)^{3/2}\mu^{-1/2} + \mathcal{O}(\mu^{-3/2})$. If $(R/h) = 5\times 10^2$ this estimate would predict a breakdown of our expansions for angles $\phi_0 \simeq 76^\circ$, while for $(R/h) = 15\times 10^2$ the corresponding value is found to be $\phi_0 \simeq 82^\circ$. It is interesting to note that the second and third terms in (5.9) become comparable for a similar asymptotic range of ϕ_0-angles; in particular, this happens for $\phi_0 \sim \pi/2 - (4\zeta_0)^{-3}\mu^{-1/2} + \mathcal{O}(\mu^{-3/2})$. Although the quantitative predictions of this latter estimate are somewhat higher than the former, it is clear that the details of the asymptotic work developed in the last two sections will have to be modified if $\phi_0 = \pi/2 - \mathcal{O}(\mu^{-1/2})$ because in that case terms such as $\tan^2\phi_0$ and $\sec^2\phi_0$, which appear in the coefficients of the equations (2.8), can no longer be regarded as $\mathcal{O}(1)$ quantities. Since now our truncated shell is very close to a full hemisphere, the use of the linear membrane basic state becomes questionable and one would normally have to account for the changes in curvature and rotations prior to the onset of the bifurcation; a nonlinear bending basic state is essential for resolving such issues. The matter is currently being pursued and the final

results will be reported elsewhere.

In keeping with Yao's [11] original study, we have confined ourselves to adopting a membrane basic state for the pre-bifurcation deformations – see (2.4). While the legitimacy of this assumption has been tried and tested in a number of previous investigations (cf. [16, 17, 24, 26]), it is not immediately obvious to what extent the asymptotic strategy used in §4 and §5 can be carried over to the case when the basic state takes into account geometrical nonlinearities. We illustrate in Figure 7 the distribution of the azimuthal and meridional pre-buckling membrane stresses, as obtained from Sanders' nonlinear shell model specialised for rotationally symmetric deformations (see Appendix B); these correspond to the blue curves shown in the left and right windows, respectively. Superimposed on those curves are the components of the basic state used in this work (plotted as dashed red curves). It is clear that the differences between the two sets of functions for $\mathring{N}_{\phi\phi}$ are minimal, and they decrease significantly as $(R/h) \gg 1$. However, the azimuthal stresses, $\mathring{N}_{\theta\theta}$, are more problematic since the presence of the boundary layers seems to qualitatively alter the earlier picture. Indeed, while the original azimuthal

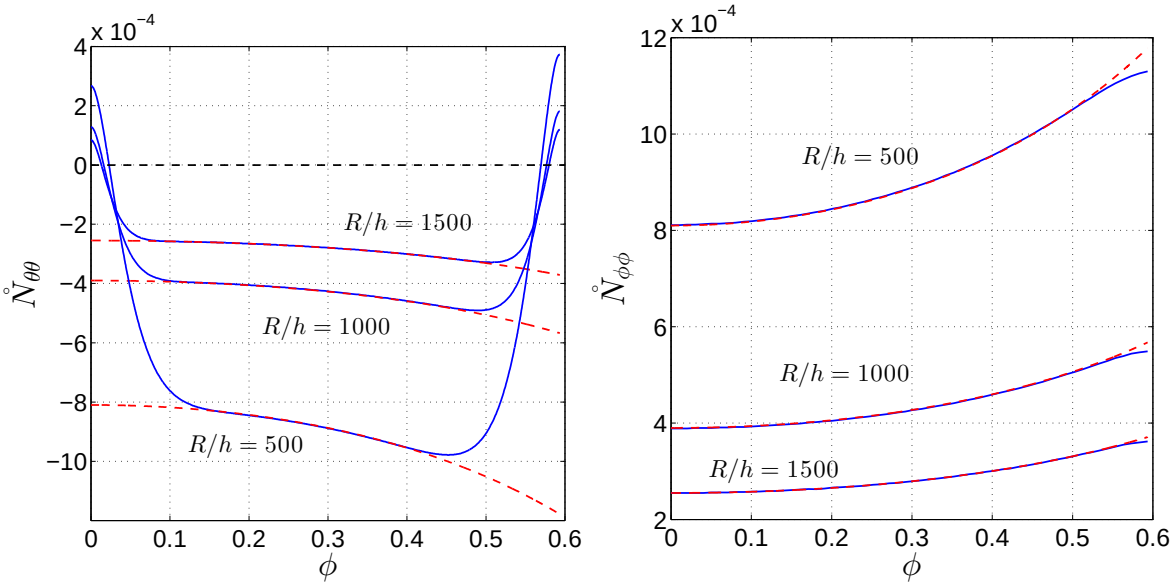

Figure 7: Comparisons between the pre-buckling membrane stresses derived from Sanders' nonlinear equations in Appendix B (continuous blue curves), and the $\pm\sec^2\phi$ expressions used in this work (dashed red curves); see main text for full explanations.

stresses were compressive throughout the shell mid-surface, Sanders' solution indicates the presence of two small *tensile* regions near the two edges ($\phi = 0$ and $\phi = \phi_0 \simeq 0.593$), with the compression being trapped inside a rather wide spherical segment contained within the lateral surface of the truncated hemisphere. The asymptotic analysis presented in this paper requires a number of non-trivial modifications in order to cope with this new scenario, and deserves further investigation.

In closing this section we return briefly to the approximation proposed by Kalamkarov and Andrianov [29]. We claim that formula (3.2) can be improved by taking advantage of the correct asymptotic structure of the bifurcation problem. For the sake of the argument we are still going to use (3.1), but will make a different choice for the "frozen" value of the angle ϕ in that equation. It has been shown in §4 that the eigenmodes reside within an $\mathcal{O}(\mu^{-1/3})$ layer attached to the rim of the truncated hemisphere, and that their leading-order part is described by the Airy-type equation (4.7). This reduced equation has a *turning* (or *transition*) point $Y_* := -\Gamma_2/\Gamma_1$ that marks the "boundary" between the

oscillatory and exponentially decaying behaviour displayed by W_0 (in the right window of Figure 4). The importance of such points in the context of stress concentration problems has been long known (e.g., see [31]), and has also been demonstrated by the present author and his associates in a number of more recent studies [1, 2, 38, 39, 40, 41]. Expressed in term of the original coordinates the foregoing turning point Y_* becomes $\phi_* := \phi_0 - \zeta_0(\mu \tan\phi_0)^{-1/3}$, which is then substituted in (3.1). With this choice the new approximation for the load parameter becomes

$$\lambda_c = 2\mu \cos^2\left[\phi_0 - \zeta_0(\tan\phi_0)^{-1/3}\mu^{-1/3}\right]. \tag{6.1}$$

The predictions (6.1) represent lower bounds for the true values of λ_c identified by numerically integrating (2.8) subject to (2.10). Two representative samples of relative errors involved in the predictions yielded by this formula are included in Figure 8; these errors range from approximately 1.5% to 4.5%, which is clearly an improvement over the results reported earlier in Figure 5 (based on reference [29]). Additional testing for many other values of ϕ_0 and $5 \times 10^2 \leq (R/h) \leq 2 \times 10^3$, not included here because of lack of space, strongly suggests that (6.1) provides much more robust estimates than the previous formula (3.2).

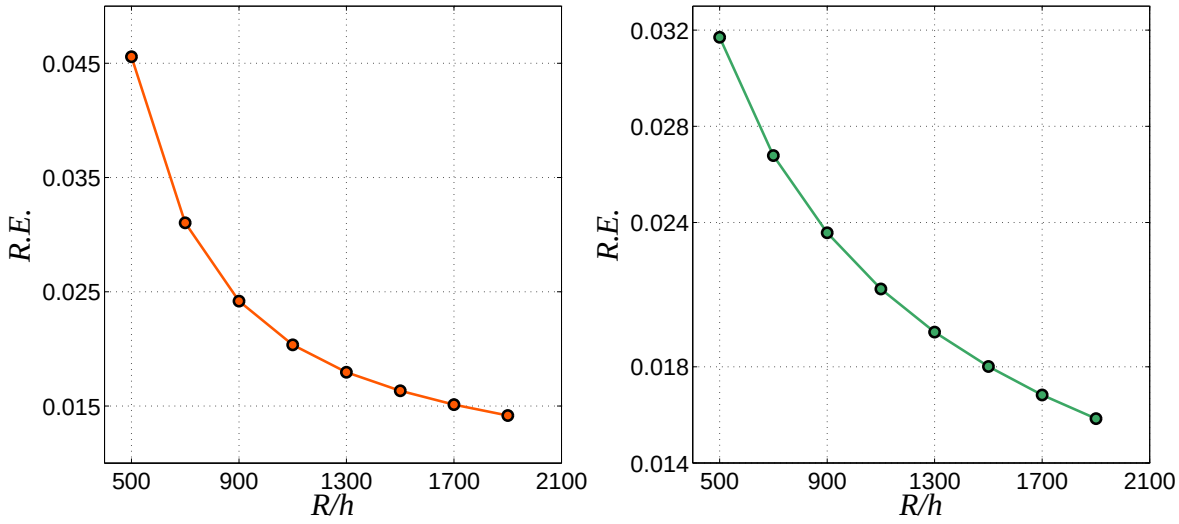

Figure 8: Relative errors (*R.E.*) for the predictions generated by the enhanced formula (6.1); on the left, $\phi_0 = 23^\circ\,30'$, while the other window shows the results for $\phi_0 = 34^\circ$. The information included in these plots is the counterpart of that from Fig. 5 (except that here we do not consider the expanded version of the new formula as well).

It is perhaps worth emphasising that this improved result (6.1) is *not* equivalent to the expansion (5.9); indeed, if we Taylor-expand the right-hand side of the former formula as $\mu \gg 1$, then the $\mathcal{O}(\mu^{1/2})$ term will be absent. Recall from §3 that the Taylor expansion of (3.2) was also missing the powers of $\mu^{1/3}$, so in a sense both results are unsatisfactory as they fail to capture the precise asymptotic structure of the full wrinkling eigenproblem. Nonetheless, both the original formula proposed in [29] and our modification of that result perform much better than normally expected and, in principle, could be used to generate orientative values for the critical loads associated with a specific shell geometry.

A Further remarks on the bifurcation equation

For the sake of completeness we include below a simple derivation of the bifurcation equation (2.1) stated earlier in the paper. The starting point is the system of nonlinear PDEs from shallow-shell theory, and which we specialise to spherical geometry (e.g., see [42])

$$D\nabla^4 w - \frac{1}{R}\nabla^2\Phi - [\Phi, w] = P\,, \tag{A.1a}$$

$$\frac{1}{Eh}\nabla^4\Phi + \frac{1}{R}\nabla^2 w + \frac{1}{2}[w, w] = 0\,. \tag{A.1b}$$

In these equations P is a pressure applied to the lateral surface of the shell (which in our case will be zero), R denotes the radius of the sphere, the bracket represents the Monge-Ampère operator defined by

$$[f, g] := (\nabla^2 f)(\nabla^2 g) - (\boldsymbol{\nabla}\otimes\boldsymbol{\nabla} f) : (\boldsymbol{\nabla}\otimes\boldsymbol{\nabla} g) \tag{A.2}$$

for any two smooth functions f and g, while the colon notation stands for the usual double-dot contracted product of second-order tensors (e.g., see [43]). The stress function Φ is related to the membrane stress tensor $\boldsymbol{N}$ according to

$$\boldsymbol{N} = (\nabla^2\Phi)\boldsymbol{I}_2 - \boldsymbol{\nabla}\otimes\boldsymbol{\nabla}\Phi\,, \tag{A.3}$$

with $\boldsymbol{I}_2$ being a suitably chosen two-dimensional identity tensor. We note in passing that the Föppl-von Kármán equations for flat plates can be obtained formally from (A.1) by taking the limit $R \to +\infty$.

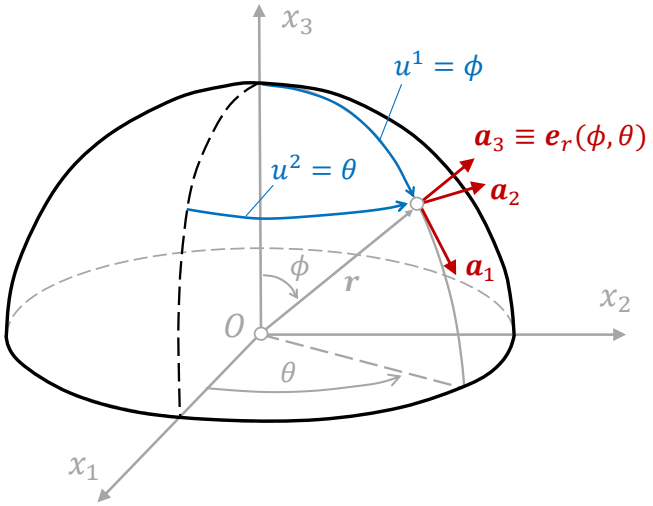

Figure 9: Upper half of a spherical surface of radius R. The location of each of its points is specified by the position vector $\boldsymbol{r} = R\boldsymbol{e}_r(\phi,\theta)$, where ϕ and θ are the angles used in the spherical coordinate system defined by the equations: $x_1 = R\sin\phi\cos\theta$, $x_2 = R\sin\phi\sin\theta$, $x_3 = R\cos\phi$, with $\phi \in [0,\pi]$ and $\theta \in [0, 2\pi)$.

The spherical surface of radius R is assumed to have a centre at the origin of the Cartesian system of coordinates, as seen in Figure 9; a point on this surface can be described by the position vector $\boldsymbol{r} = R\boldsymbol{e}_r(\phi,\theta)$. The two angles ϕ and θ in the spherical coordinate system (r,ϕ,θ) are selected as

surface coordinates, and we introduce the notations: $u^1 := \phi$ and $u^2 := \theta$, so that any point on the sphere can be represented by the position vector $\boldsymbol{r} = \boldsymbol{r}(u^1, u^2)$. The definition of θ and ϕ in Figure 9 is slightly at odds with the standard conventions usually encountered in the literature (where $\theta \to \varphi$ and $\phi \to \theta$). Furthermore, we recall from §2 (see Figure 2) that our ϕ is actually the complement of the one chosen here. In the interest of clarity we shall use the definitions recorded in Figure 9 and only at the end we shall make the substitution $\phi \to \pi/2 - \phi$ in order to recover the form of the equations stated in the earlier parts of this study.

The covariant base vectors in the middle surface of the sphere are then $\boldsymbol{a}_\alpha = \boldsymbol{r}_{,\alpha}$ ($\alpha = 1, 2$), the comma notation being used to denote partial derivatives with respect to u^α; more specifically, $\boldsymbol{a}_1 = R\,\boldsymbol{e}_\phi$ and $\boldsymbol{a}_2 = R\sin\phi\,\boldsymbol{e}_\theta$, and the covariant components of the metric tensor ($a_{\alpha\beta} \equiv \boldsymbol{a}_\alpha \cdot \boldsymbol{a}_\beta$) are found to be $a_{11} = R^2$, $a_{12} = a_{21} = 0$, $a_{22} = R^2\sin^2\phi$. The contravariant base vectors are easily identified as $\boldsymbol{a}^1 = \boldsymbol{e}_\phi/R$ and $\boldsymbol{a}^2 = \boldsymbol{e}_\theta/(R\sin\phi)$. Thus, the contravariant components of the metric tensor ($a^{\alpha\beta} \equiv \boldsymbol{a}^\alpha \cdot \boldsymbol{a}^\beta$) are simply $a^{11} = 1/R^2$, $a^{12} = a^{21} = 0$, $a^{22} = 1/(R^2\sin^2\phi)$, and the Christoffel symbols turn out to be identically zero, except for $\Gamma^2_{12} \equiv \Gamma^2_{21} = \cot\phi$ and $\Gamma^1_{22} = -\sin\phi\cos\phi$.

With this background in mind, the surface gradient operator is

$$\boldsymbol{\nabla} \equiv \boldsymbol{a}^\alpha \frac{\partial}{\partial u^\alpha} \equiv \frac{1}{R}\left(\boldsymbol{e}_\phi \frac{\partial}{\partial\phi} + \boldsymbol{e}_\theta \frac{1}{\sin\phi}\frac{\partial}{\partial\theta}\right),$$

while the Laplace-Beltrami operator of a *surface* scalar field $\varphi \equiv \varphi(u^1, u^2)$ is given by the usual formula, $\nabla^2\varphi = a^{\alpha\beta}\nabla_\alpha\varphi_{,\beta}$. Here, $\nabla_\alpha c_\beta \equiv c_{\beta,\alpha} - \Gamma^\gamma_{\alpha\beta}c_\gamma$ represents the covariant derivative of the the covariant components (c_β) of a surface vector field $\boldsymbol{c} = c_\beta\boldsymbol{a}^\beta$; in our particular case of a spherical surface it is found that

$$\nabla^2 = \frac{1}{R^2}\left(\frac{\partial^2}{\partial\phi^2} + \cot\phi\frac{\partial}{\partial\phi} + \frac{1}{\sin^2\phi}\frac{\partial^2}{\partial\theta^2}\right). \tag{A.4}$$

To find possible bifurcations from a known rotationally symmetric solution $\mathring{w} \equiv \mathring{w}(\phi)$ and $\mathring{\Phi} \equiv \mathring{\Phi}(\phi)$ of (A.1), we can employ the method of adjacent equilibrium. This involves considering perturbations of the form $w(\phi,\theta) \to \mathring{w}(\phi) + \widehat{w}(\phi,\theta)$ and $\Phi(\phi,\theta) \to \mathring{\Phi}(\phi) + \widehat{\Phi}(\Phi,\theta)$, that are then substituted in (A.1), followed by the linearisation of the resulting equations. Taking into account that the Monge-Ampère operator is a bilinear mapping and the symmetric basic state satisfies the same equations, the outcome of the aforementioned manipulations can be shown to be

$$D\nabla^4\widehat{w} - \frac{1}{R}\nabla^2\widehat{\Phi} - [\mathring{\Phi}, \widehat{w}] - [\widehat{\Phi}, \mathring{w}] = 0\,, \tag{A.5a}$$

$$\frac{1}{Eh}\nabla^4\widehat{\Phi} + \frac{1}{R}\nabla^2\widehat{w} + [\mathring{w}, \widehat{w}] = 0\,. \tag{A.5b}$$

All that is left to do now is evaluate the square-bracket terms in (A.5) as well as the membrane stress tensor given in (A.3). A close look at the expressions recorded above suggests we start with the Hessian operator $\boldsymbol{\nabla}\otimes\boldsymbol{\nabla}$. Note that, for example, $\boldsymbol{\nabla}\otimes\boldsymbol{\nabla}\widehat{\Phi} = \big(\nabla_\alpha\widehat{\Phi}_{,\beta}\big)\boldsymbol{a}^\alpha\otimes\boldsymbol{a}^\beta$, and this last formula can be expressed in terms of $\boldsymbol{e}_\phi$ and $\boldsymbol{e}_\theta$ (according to what has already been said above). The results for $\mathring{\Phi}$ and $\widehat{\Phi}$ are recorded below,

$$\begin{aligned}\boldsymbol{\nabla}\otimes\boldsymbol{\nabla}\widehat{\Phi} = \frac{1}{R^2}\left(\frac{\partial^2\widehat{\Phi}}{\partial\phi^2}\right)\boldsymbol{e}_\phi\otimes\boldsymbol{e}_\phi + \frac{1}{R^2\sin\phi}\left(\frac{\partial^2\widehat{\Phi}}{\partial\phi\partial\theta} - \cot\phi\,\frac{\partial\widehat{\Phi}}{\partial\theta}\right)(\boldsymbol{e}_\phi\otimes\boldsymbol{e}_\theta + \boldsymbol{e}_\theta\otimes\boldsymbol{e}_\phi)\\ + \frac{1}{R^2}\left(\frac{1}{\sin^2\phi}\frac{\partial^2\widehat{\Phi}}{\partial\theta^2} + \cot\phi\,\frac{\partial\widehat{\Phi}}{\partial\phi}\right)\boldsymbol{e}_\theta\otimes\boldsymbol{e}_\theta\,,\end{aligned} \tag{A.6}$$

$$\boldsymbol{\nabla}\otimes\boldsymbol{\nabla}\mathring{\Phi}=\frac{1}{R^2}\left(\frac{\partial^2\mathring{\Phi}}{\partial\phi^2}\right)\boldsymbol{e}_\phi\otimes\boldsymbol{e}_\phi+\frac{\cot\phi}{R^2}\left(\frac{d\mathring{\Phi}}{d\phi}\right)\boldsymbol{e}_\theta\otimes\boldsymbol{e}_\theta\,; \tag{A.7}$$

the corresponding Hessians for $\widehat{w}$ and $\mathring{w}$ are obtained, respectively, from (A.6) and (A.7) by making the obvious substitutions. Thus, by evaluating the terms in (A.2), we eventually discover

$$[\mathring{\Phi},\widehat{w}]=\frac{1}{R^2}\left[\frac{\cot\phi}{R^2}\left(\frac{d^2\mathring{\Phi}}{d\phi^2}\right)\frac{\partial\widehat{w}}{\partial\phi}+\frac{1}{R^2\sin^2\phi}\left(\frac{d^2\mathring{\Phi}}{d\phi^2}\right)\frac{\partial^2\widehat{w}}{\partial\theta^2}+\frac{\cot\phi}{R^2}\left(\frac{d\mathring{\Phi}}{d\phi}\right)\frac{\partial^2\widehat{w}}{\partial\phi^2}\right], \tag{A.8}$$

and a similar expression holds for $[\widehat{\Phi},\mathring{w}]$ (by changing $\widehat{w}\to\widehat{\Phi}$ and $\mathring{w}\to\mathring{\Phi}$). The expression (A.8) can be simplified by replacing the pre-buckling one-dimensional fields in terms of the components of the membrane stress tensor. Use of (A.3) with $\Phi\to\mathring{\Phi}$ with $\boldsymbol{I}_2=\boldsymbol{e}_\phi\otimes\boldsymbol{e}_\phi+\boldsymbol{e}_\theta\otimes\boldsymbol{e}_\theta$ gives

$$\mathring{\boldsymbol{N}}=\frac{\cot\phi}{R^2}\left(\frac{d\mathring{\Phi}}{d\phi}\right)\boldsymbol{e}_\phi\otimes\boldsymbol{e}_\phi+\frac{1}{R^2}\left(\frac{d^2\mathring{\Phi}}{d\phi^2}\right)\boldsymbol{e}_\theta\otimes\boldsymbol{e}_\theta\,, \tag{A.9}$$

and then (A.8) becomes

$$[\mathring{\Phi},\widehat{w}]=\frac{1}{R^2}\left[\mathring{N}_{\phi\phi}\,\frac{\partial^2\widehat{w}}{\partial\phi^2}+\mathring{N}_{\theta\theta}\,\mathcal{L}(\widehat{w})\right], \tag{A.10}$$

after we remember to make the substitution $\phi\to\pi/2-\phi$; the operator $\mathcal{L}$ was defined in (2.2b). Similarly, for the other square-bracket term in (A.5a) we find

$$[\widehat{\Phi},\mathring{w}]=\frac{1}{R^4}\left[\left(\frac{d^2\mathring{w}}{d\phi^2}\right)\mathcal{L}(\widehat{w})-\tan\phi\left(\frac{d\mathring{w}}{d\phi}\right)\frac{\partial^2\widehat{\Phi}}{\partial\phi^2}\right]. \tag{A.11}$$

On substituting (A.10) and (A.11) back into (A.5a), and recalling that $\nabla^2=R^{-2}\nabla_*^2$, equation (2.6a) follows quickly after multiplying the resulting expressions by R^4. The second equation in the system (2.6) is obtained by employing the same strategy, and we omit the details in the interest of brevity. The presence of the $\mathring{w}$-terms in (2.1) – see (A.10) and (A.11) above, reflects the fact that the shell mid-surface before and after deformation cannot be identified; such terms become important when the bending of the basic state is taken into consideration.

Since we changed the representation of our shell equations by using the latitude angle ϕ (rather than the more usual co-latitude angle), some care must be taken with the mecahnical interpretation of the various fields in our eigenproblem. It is clear that by making this change the direction of $\boldsymbol{a}_1$ is reversed, so the original local system of coordinates becomes left-handed. To get back to a right-handed system we can, for example, reverse the direction of $\boldsymbol{a}_3$ as well. If this change is made then positive transverse displacements represent displacements towards the geometrical centre of the sphere; another option would be to reverse the direction of $\boldsymbol{a}_2$, which is equivalent to $\theta\to-\theta$. Finally, we remark in passing that the equations (2.6) are invariant under the transformation $(\widehat{w},\widehat{\Phi})\to(-\widehat{w},-\widehat{\Phi})$.

B Basic state based on Sanders' kinematics

We refer to the original paper [25] for a full account of this highly regarded shell theory. Our interest here is in a simplified version known as 'small strain–moderate rotation theory'. The extensional and shearing strain components in the shell mid-surface are assumed to remain small, but rotations are allowed to be *moderately small*, a concept that is fully explained in the aforementioned reference.

Most nonlinear shell theories that lend themselves to some form of analytical work are based on this assumption.

The spherical coordinates of the previous section are still in use, and the following notations are employed below: the displacements in the direction $\boldsymbol{e}_\phi$, $\boldsymbol{e}_\theta$ and $\boldsymbol{e}_r$ are denoted by u, v and w, respectively; β_ϕ and β_θ are the rotations along the ϕ and θ coordinate directions, while χ_ϕ and χ_θ represent flexural curvature changes of the surface in the ϕ and θ directions; $\chi_{\phi\theta}$ corresponds to the flexural twist of the surface. All these quantities depend on the displacements of the mid-surface through some nonlinear kinematics relationships (that are readily available in [25]). The forces ($N_{\alpha\gamma}$ for α, $\gamma \in \{\phi, \theta\}$), the moments ($M_{\alpha\gamma}$ for α, $\gamma \in \{\phi, \theta\}$), and the transverse shear forces ($Q_{\phi r}$ and $Q_{\theta r}$) per unit length of the shell satisfy a number of equilibrium equations. In addition, the constitutive equations relate the $N_{\alpha\gamma}$ to the extensional and shearing strain components ($\varepsilon_{\alpha\gamma}$); the moments $M_{\alpha\gamma}$ are related to the curvature changes (χ_α for $\alpha \in \{\phi, \theta\}$ – also known as bending strains).

For rotationally symmetric deformations, $\mathring{v} \equiv 0$, $\mathring{\beta}_\theta \equiv 0$, $\mathring{\beta} \equiv 0$, $\mathring{\chi}_{\phi\theta} \equiv 0$, $\mathring{M}_{\phi\theta} \equiv 0$, $\mathring{N}_{\phi\theta} \equiv 0$, etc, and all the remaining quantities depend only on the meridional coordinate ϕ (the superimposed "dot" referes to pre-buckling fields). It can be shown that in this scenario Sanders' equations can be cast in the convenient form

$$\frac{d\boldsymbol{y}}{d\phi} = \boldsymbol{f}(\phi, \boldsymbol{y}(\phi))\,, \qquad 0 < \phi < \phi_0\,, \tag{B.1}$$

where $\boldsymbol{y}$ and $\boldsymbol{f}$ are 6×1 vectors, with components

$$y_1 \equiv \mathring{u}(\phi)\,, \qquad y_2 \equiv \mathring{w}(\phi)\,, \qquad y_3 \equiv \mathring{\beta}_\phi(\phi)\,,$$
$$y_4 \equiv \mathring{N}_{\phi\phi}(\phi)\,, \qquad y_5 \equiv \mathring{Q}_{\phi r}(\phi)\,, \qquad y_6 \equiv \mathring{M}_{\phi\phi}(\phi)\,,$$

and

$$f_1 := y_4 - (1+\nu)y_2 + (\nu\tan\phi)y_1 - \frac{1}{2}y_3^2\,, \quad f_2 := y_1 - y_3\,, \quad f_3 := y_6 + (\nu\tan\phi)y_3\,,$$

$$f_4 := \tan\phi\left(\frac{1-\nu-\nu^2}{1-\nu^2}\right)y_4 - (y_2 - y_1\tan\phi)\tan\phi - y_5 + y_3y_4\,,$$

$$f_5 := (\tan\phi - y_3)y_5 + \left[\left(\frac{1+\nu-\nu^2}{1-\nu^2}\right) - \left(\frac{\nu^3\tan\phi}{1-\nu^2}\right)y_3 + y_3^2\right]y_4$$
$$+(1 - y_3\tan\phi)(y_2 - y_1\tan\phi) + y_4y_6\,,$$

$$f_6 := [(1-\nu)\tan\phi]\,y_6 + \left[(1-\nu^2)\tan^2\phi\right]y_3 + \mu^2 y_5\,.$$

The choice of the above dependent variables is motivated by the expressions that appear in the boundary conditions for an edge ϕ =constant. According to [25] such boundary constraints involve specifying

$$\text{(i) } \mathring{N}_\phi \quad \text{or} \quad \mathring{u}; \qquad \text{(ii) } \mathring{Q}_{\phi r} \quad \text{or} \quad \mathring{w}; \quad \text{(iii) } \mathring{M}_{\phi\phi} \quad \text{or} \quad \mathring{\beta}_\phi\,. \tag{B.2}$$

To mimic the particular edge restraints relevant to the problem in §2 we follow [26] and take

$$\mathring{u} = \mu^{-1}\Delta\cos\phi_0\,, \quad \mathring{w} = \mu^{-1}\Delta\sin\phi_0\,, \quad \mathring{\beta}_\phi = 0\,, \qquad \text{for} \quad \phi = \phi_0\,,$$

while the rigid clamping of the lower edge translates into

$$\mathring{u} = \mathring{w} = \mathring{\beta}_\phi = 0\,, \qquad \text{for} \quad \phi = 0\,.$$

The quantity $\Delta > 0$ above represents a controlled vertical displacement and serves as the loading parameter in the nonlinear shell model described by (B.1). To find the vertical force that is responsible for the deformation produced by imposing such a prescribed value of Δ one can simply compute $\mathring{N}_{\phi\phi}$ at the equatorial edge ($\phi = 0$). In the left window of Figure 7 the dashed red curves are obtained by plotting $\mathring{N}_{\phi\phi}(\phi = 0) \times (-\sec^2\phi)$, while their counterparts in the right window correspond to the negative of this expression – see equations (2.4) as well. The value of Δ is that corresponding to a bifurcation associated with this new basic state; however, in Figure 7 we kept $\Delta \simeq 0.7$ constant and increased (R/h) in order to illustrate the "convergence" of the nonlinear basic state to our original choice mentioned in §2. In a true eigenvalue problem the critical size of the imposed vertical displacement associated with an instability is determined by the particular structure of the bifurcation equations. We have carried out a detailed numerical analysis of the full bifurcation equations from Appendix A together with either (B.1) or a nonlinear shallow-shell basic state, but will postpone an in-depth discussion of the relevant results until the asymptotic analyses of the corresponding problems are also completed.

References

[1] Coman, C.D., Haughton, D.M.: Localized wrinkling instabilities in radially stretched annular thin films. Acta Mech. **185**, 179–200 (2006)

[2] Coman, C.D., Bassom, A.P.: On the wrinkling of a pres-stressed annular thin film in tension. J. Mech. Phys. Solids **55**, 1601–1617 (2007)

[3] Davidovitch, B., Scholl, R.D., Vella, D., Adda-Bedia, M., Cerda, E.A.: Prototypical model for tensional wrinkling in thin sheets. Proceedings of the National Academy of Sciences of the USA **108**, 18277-18232 (2011)

[4] Damil, N., Potier-Ferry, M., Hu, H.: Membrane wrinkling revisited from a multiscale point of view. Advanced Modelling and Simulation in Engineering Science **1**, 6 (2014)

[5] Taylor, M., Davidovitch, B., Qiu, Z., Bertoldi, K.: A comparative analysis of numerical approaches to the mechanics of thin elastic sheets. Journal of the Mechanics and Physics of Solids **79**, 92-107 (2015)

[6] Liu, X.., Liu, Y: Radial instabilities of viscoelastic thin film-elastic substrate system triggered by local prestretch: a theoretical solution. Mechanics of Materials **143**, 103315 (2020)

[7] Geminard, J-C., Bernal, R., Melo, F.: Wrinkle formation in axi-symmetrically stretched membranes. European Physics Journal E: Soft Matter **15**, 117-126 (2004)

[8] Genzer, J., Groenewold, J.: Soft matter with hard skin: from skin wrinkles to templating and material characterization. Soft Matter **3**, 310-323 (2006)

[9] Wang, C, Liu, Y., Lan. L., Tan, H.: Graphene wrinkling: formation, evolution and collapse. Nanoscale **5**, 4454-4461 (2013)

[10] Wang, C., Lan. L., Tan, H.: The physics of wrinkling in graphene membranes under local tension. Physical Chemistry Chemical Physics **15**, 2764-2773 (2013)

[11] Yao, J.C.: Buckling of a truncated hemisphere under axial tension. AIAA Journal **1**, 2316-2319 (1963)

[12] Brush, Don O., Almroth, Bo O.: Buckling of Bars, Plates and Shells. McGraw-Hill Book Company, New York (1975)

[13] Troger, H., Steindl, A.: Nonlinear Stability and Bifurcation Theory. Springer-Verlag, Wien (1991)

[14] Flügge, W.: Stresses in Shells. Springer-Verlag, Berlin (1973)

[15] Gould, P.L.: Analysis of Plates and Shells. Prentice Hall, Upper Saddle River, New Jersey (1999)

[16] Bushnell, D.: Bifurcation phenomena in spherical shells under concentrated and ring loads. AIAA Journal **5**, 2034–2040 (1967)

[17] Bushnell, D.: Computerized Buckling Analysis of Shells. Kluwer Academic Publishers, Dordrecht (1989)

[18] Reissner, E.: On axisymmetric deformations of thin shells of revolution. In : *Proceedings of the Third Symposium in Applied Mathematics. Vol III: Elasticity*, R.V. Churchill, E. Reissner, A.H. Taub (Eds.), 27–52. McGraw-Hill Company; New York, 1950.

[19] Bushnell, D.: Nonlinear axisymmetric behavior of shells of revolution. AIAA Journal **5**, 432–439 (1966)

[20] Bushnell, D.: Symmetric and nonsymmetric buckling of finitely deformed eccentrically stiffened shells of revolution. AIAA Journal **5**, 1455–1462 (1967)

[21] Budiansky, B., Hutchinson, J.W.: A survey of some buckling problems. AIAA Journal **4**, 1505–1510 (1966)

[22] Hutchinson, J.W.: Initial post-buckling behavior of toroidal shell segments. Int. J. Solids Structures **3**, 97–115 (1967)

[23] Navaratna, D.R., Pian, T.H.H., Witmer, E.A.: Stability analysis of shells of revolution by the finite element method. AIAA Journal **6**, 355–361 (1968)

[24] Wu, M.T., Cheng, S.: Nonlinear asymmetric buckling of truncated spherical shells. ASME J. Appl. Mech. **37**, 651–660 (1970)

[25] Sanders, J.L. Jr.: Nonlinear theories for thin shells. Quart. Appl. Math. **6**, 21–36 (1963)

[26] Radhamohan, S.K., Prasad, B.: Asymmetric buckling of toroidal shells under axial tension. AIAA Journal **12**, 511–515 (1974)

[27] Bagchi, A.: Linear and nonlinear buckling of thin shells of revolution. Trends in Applied Sciences Research **7**, 196–209 (2012)

[28] Shilkrut, D.: Stability of Nonlinear Shells. Elsevier, Amsterdam, The Netherlands (2002)

[29] Kalamkarov, A.L, Andrianov, I.I.: Analytical solution of the stability problem for the truncated hemispherical shell under tensile loading. Mathematical Problems in Engineering. **2018**, article ID: 5260639 (2018)

[30] Singer, J., Arbocz, J., Weller, T.: Buckling Experiments (Vol. 2). John Wiley & Sons, New York (2002)

[31] Steele, C.R.: Application of the WKB method in solid mechanics. In : *Mechanics Today, Vol. 3*, S. Nemat-Nasser (Ed.), 243–295. Pergamon Press; New York, 1976.

[32] Fu, Y.B.: Some asymptotic results concerning the buckling of a spherical shell of arbitrary thickness. International Journal of Non-Linear Mechanics 1998; 33: 1111–1122.

[33] Jakobsen, A.A.: Beitrag zur Theorie der Kugelschale auf Einzelstütze. Ingenieur-Archiv **8**, 275–294 (1937)

[34] Coman, C.D.: Oval cylindrical shells under asymmetric bending: a singular-perturbation solution. Zeitschrift für Angewandte Mathematik und Physik **69:120** (2018)

[35] Coman, C.D.: Remarks on elastic buckling for sectorial plates. Int. J. Eng. Sci. **47**, 1002–1013 (2009)

[36] Coman, C.D., Bassom, A.P.: Wrinkling structures at the rim of an initially stretched circular thin plate subjected to transverse pressure. SIAM Journal of Applied Mathematics **78**, 1009–1029 (2018)

[37] Coman, C.D., Matthews, M.T., Bassom, A.P.: Asymptotic phenomena in pressurised thin films. Proceedings of the Royal Society of London A **471**, 20150471 (2015)

[38] Coman, C.D., Bassom, A.P.: Wrinkling of pre-stressed annular thin films under azimuthal shearing. Mathematics and Mechanics of Solids **13**, 513–531 (2008)

[39] Coman, C.D.: Asymptotic approximations for pure bending of thin cylindrical shells. Zeitschrift für Angewandte Mathematik und Physik **68:82** (2017)

[40] Coman, C.D.: Some applications of the WKB method to the wrinkling of bi-annular plates in tension. Acta Mech. **224**, 399–423 (2013)

[41] Coman, C.D.: On the asymptotic reduction of the Föppl-von Kármán bifurcation system for an edge-buckling instability. Acta Mech. **229**, 1099–1109 (2018)

[42] Coman, C.D., Bassom, A.P.: Asymptotic limits and wrinkling patterns in a pressurised shallow spherical cap. International Journal of Non-linear Mechanics **81**, 8–18 (2016)

[43] Coman, C.D.: Continuum Mechanics and Linear Elasticity: An Applied Mathematics Introduction. Springer Nature B.V., Dordrecht (2020)